Study of the Effects of Progressive Changes in Alkoxysilane Structure on Sol−Gel Reactivity

Bing Tan[†] and Stephen E. Rankin*

Department of Chemical & Materials Engineering, University of Kentucky, 177 Anderson Hall, Lexington, Kentucky 40506-0046

Received: January 18, 2006; In Final Form: July 17, 2006

Effects of the structure of an alkoxysilane on the early reaction kinetics of sol−gel polymerization are investigated in basic and acidic conditions. Six silanes, including tetraethoxysilane (TEOS), tetramethoxysilane (TMOS), methyltrimethoxysilane (MTMS), bis(trimethoxysilyl)ethane (BTMSE), bis(trimethoxysilyl)hexane (BTMSH), and bis(trimethoxysilylpropyl)amine (BTMSPA), are selected to examine the effects of progressive changes in the silane's structure. In basic conditions, reactivities of the silanes follow the pairwise trends TEOS ≪ TMOS, TMOS > MTMS, MTMS < BTMSE, BTMSE ≫ BTMSH, and BTMSH ≪ BTMSPA. Hydrolysis rate coefficients of BTMSE, TMOS, MTMS, and BTMSPA are similar in value and are almost one order of magnitude larger than the coefficients of BTMSH and TEOS. In acidic conditions, the pairwise reactivity trends are TEOS ≈ TMOS, TMOS < MTMS, MTMS > BTMSE, BTMSE ≫ BTMSH, and BTMSH > BTMSPA. The condensation rate coefficients of BTMSH and BTMPA are much smaller than the others. Theses relationships can be explained mainly on the basis of the expected inductive and steric factors of the silanes. Bulky organics attached to the silane lead to low reactivity in both acidic and basic conditions. A high electron density at silicon leads to a low reactivity in basic conditions but a high reactivity in acidic conditions (pH ∼2.3). Only BTMSPA in basic conditions defies these trends, possibly because of the effects of solvation near the reactive silicon site.

Introduction

The sol−gel method of ceramic synthesis has been known for hundreds of years but has recently become a widespread and developing method of forming nanostructured materials.[1] This process is defined as the polymerization of inorganic precursors to produce a sol, which eventually grows into a metal oxide gel network. Equations 1−4 illustrate the sequence of functional group sol−gel reactions of an alkoxysilane precursor, which consists of reversible hydrolysis (eqs 1 and 2) and water-producing (eq 3) or alcohol-producing (eq 4) condensation. Condensation may be reversible under some conditions as well, but early in the process, reversibility can be neglected.

$$\mathrm{Si{-}OR + H_2O \xrightarrow{k_h} Si{-}OH + ROH} \quad (1)$$

$$\mathrm{Si{-}OH + ROH \xrightarrow{k_h'} Si{-}OR + H_2O} \quad (2)$$

$$\mathrm{Si{-}OH + HO{-}Si \xrightarrow{k_{cw}} Si{-}O{-}Si + H_2O} \quad (3)$$

$$\mathrm{Si{-}OH + RO{-}Si \xrightarrow{k_{ca}} Si{-}O{-}Si + ROH} \quad (4)$$

Because these reactions proceed near ambient conditions, it is possible to incorporate organic components into sol−gel ceramics by three routes. First, supramolecular templates such as surfactants can be introduced.[2,3] These templates self-assemble into molecular aggregates that physically assemble with silicates through Si−OH or Si−O$^-$ groups.[4−7] The surfactants can be retained to create organic−inorganic hybrids or removed to generate mesoporous products. The second method of introducing organic components is by replacing one, two, or three alkoxysilane groups of the precursor with nonhydrolyzable organics (for instance, by using methyltrimethoxysilane).[8−11] This will lead to materials with dangling, or nonbridging, organics. The third method is to use a bridged silane, which is a precursor with two trialkoxysilyl moieties joined by an organic segment (for instance, 1,2-bis(trimethoxysilyl) ethane).[12,13]

All three methods of organic modification are useful for controlling some aspect of the structure and properties of a sol−gel material. Surfactant incorporation is an excellent method of introducing an organic component with long-range order. Because the interactions with the material are only physical, the surfactant can also be easily extracted to generate a mesoporous material. Nonbridging organics are covalently incorporated into the material structure and can be used to introduce specialized functionality or to modify the surface properties of the material. A wide variety of organotrialkoxysilanes is available for this purpose. However, siloxane cyclization may limit the ability of these organotrialkoxysilanes to form networks.[14,15] Bridged silanes overcome this limitation because they gel much more easily than trifunctional alkoxysilanes do.[12,13] They also introduce organic components directly into the gel network without blocking the accessibility of the pores that are obtained after drying.

Recently, there have been several demonstrations of combining these methods of organic modification to create advanced materials with combinations of useful properties. For instance, using bridged silanes with surfactant templates leads to mesoporous organic−inorganic hybrid materials with highly acces-

* To whom correspondence should be addressed. Tel: (859) 257-9799. Fax: (859) 323-1929. E-mail: srankin@engr.uky.edu.

[†] Current address: Chemistry Department, Ohio State University, Columbus, OH.

10.1021/jp060376k CCC: $33.50
Published on Web 10/19/2006

sible pores.[16−18] In other examples, several bridged and nonbridged silanes are combined to create multifunctional "smart" hybrid materials.[19−22] There are also many situations in which tetraalkoxysilanes and organo-trialkoxysilanes are combined to tune the properties and network-forming ability of a material.[11,23] To better understand and control these types of mixed systems, we need to understand the effects of silane modification on the kinetics and interactions among components. In this paper, we systematically investigate a series of alkoxysilanes to separate the effects of different types of organic modification on the reaction kinetics.

Regardless of the type of precursor used, the relevant functional-group reactions are the hydrolysis and condensation illustrated in eqs 1−4.[24] Depending on the reaction conditions, different reactions are rate-controlling. In basic conditions, hydrolysis has been shown to be the rate-limiting step.[25−27] On the other hand, in acidic conditions, condensation reactions are rate-limiting.[25,27−29] Both types of conditions are relevant to the synthesis of ordered mesoporous materials; both alkaline and acidic conditions are used for the precipitation of surfactant/(organo)siloxane aggregates from mostly aqueous solutions,[30−36] and acidic alcohol/water solvents are typically used to prepare thin films,[37−42] aerosol particles,[43] and monoliths.[44,45]

Whatever the synthesis method, knowledge of the kinetics of the sol−gel reactions helps to control the structure of the resulting material. When a single precursor is used, there is a competition between the rate of the sol−gel reactions and the rates of mesophase formation and (when dilute solutions are used) precipitation.[46−52] The rate of hydrolysis and polycondensation can determine whether a solid network is able to form before or after an ordered mesophase forms or precipitation begins. Differences in precursor reactivity have been hypothesized to play a significant role in determining the range of conditions in which ordered organically functionalized materials can be synthesized.[53] It is even more important to understand the effect of precursor structure on reactivity when cocondensation of different alkoxysilanes is used to control the amount(s) of different organic functional groups.[11,19−23,54−57] It is not unusual for prehydrolysis procedures to be used to control homogeneity of the functional groups,[1,19,37,52,54] and knowing precursor kinetics allows for good design of these procedures.

To measure meaningful rate coefficients, kinetic studies of the sol−gel reactions must be carried out in homogeneous solutions with well-defined species concentrations. To achieve these conditions, we must add enough alcohol to mix the precursors and water immediately after mixing (because alkoxides are hydrophobic prior to hydrolysis). The amount of water also must be limited to avoid early precipitation with some silanes, and kinetic studies must be carried out in the absence of surfactants to avoid micellization and microphase separation. The conditions of the kinetic studies are directly applicable (with consideration of activity coefficient effects) to synthetic methods that utilize homogeneous sols up until the point that the material forms; this includes all of the traditional routes to homogeneous films, fibers, monoliths, and aerosol particles.[30,31,58] These kinetic studies are also relevant to the reactions that occur in precipitating systems,[1,59−63] but will need to be supplemented with investigations of phase stability, species partitioning between phases, and mesophase crystallization rates.

The effects of the type and number of alkoxide groups and the length and type of functional groups on the sol−gel reaction have been investigated under homogeneous reaction conditions.[1,60] Effects of steric and inductive factors in tetrafunctional and trifunctional alkoxysilanes have been reviewed.[64,65] However, comparisons of the kinetics of nonbridged silanes with their corresponding bridged silanes and among bridged silanes with different bridging organics have not been made. In fact, bridged silanes have only rarely been the subject of any sort of kinetic investigation.[63,66,67]

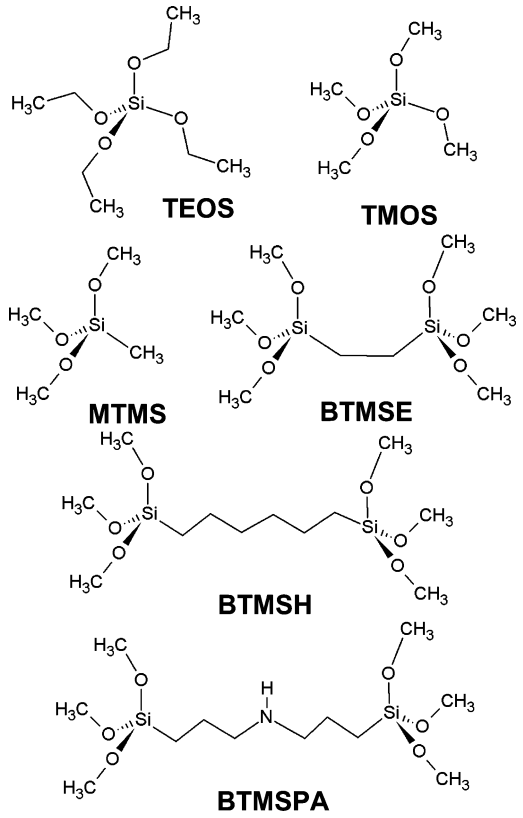

Figure 1. Structure of the alkoxysilane precursors studied here.

Here, we investigate a series of silanes in which structural and chemical differences are gradually introduced. We will measure the early reaction kinetics of tetraethoxysilane (TEOS), tetramethoxysilane (TMOS), methyltrimethoxysilane (MTMS), 1,2-bis(trimethoxysilyl)ethane (BTMSE), 1,6-bis(trimethoxysilyl)hexane (BTMSH), and bis(trimethoxysilylpropyl)amine (BTMSPA). These six precursors are illustrated in Figure 1. The difference between TEOS and TMOS is the size of the alkoxide. When one of the methoxy groups in TMOS is substituted with a methyl group, the resulting molecule is MTMS. Whereas TMOS has four functional groups capable of being hydrolyzed and condensed, MTMS has only three hydrolyzable groups. BTMSE can be thought of as a bridged silane formed by joining together two MTMS molecules. The effect of the length of the bridging chain can be observed by comparing BTMSE (two carbons in the bridging chain) to BTMSH (six carbons in the bridging chain). The final member in this series, BTMSPA, has a bridging chain with six carbons and one amine. Thus, the main difference between BTMSPA and BTMSH is the amine functional group located at the center of the BTMSPA chain. All the bridged silanes used here have six hydrolyzable functional groups. With this series of silanes, we will relate kinetic differences to structural differences, including the size of alkoxide, functionality of the precursor, length of the organic group, and bridging by the organic. This fundamental kinetic information will allow for the application of chemical reaction engineering principles to optimizing

TABLE 1. Rate Coefficients Found for the Sol−Gel Reaction in Basic Conditions

sample	precursor	k_{h1}[a] ($\times 10^{-3}$ M^{-1} s^{-1})	k_{h2}[b] ($\times 10^{-3}$ M^{-1} s^{-1})
B1	TEOS	0.293 ± 0.004	
B2	TMOS	2.35 ± 0.03	2.70 ± 0.03
B3	MTMS	1.97 ± 0.01	1.71 ± 0.02
B4	BTMSE	2.69 ± 0.03	2.28 ± 0.02
B5	BTMSH	0.305 ± 0.004	0.323 ± 0.007
B6	BTMSH	0.369 ± 0.007	0.28 ± 0.01
B7	BTMSPA	1.54 ± 0.02	1.61 ± 0.01

[a] k_{h1}: Calculated from the $SiOCH_3$ band intensity. [b] k_{h2}: Calculated from the H_2O band intensity.

TABLE 2. Rate Coefficients Founds for the Sol−Gel Reaction in Acidic Conditions

sample	precursor	$k_{ac}{}^1$[a] ($\times 10^{-4}$ M^{-1} s^{-1})	$k_{ac}{}^2$[b] ($\times 10^{-4}$ M^{-1} s^{-1})
A1	TEOS		
A2	TMOS	1.08 ± 0.09	
A3	MTMS	3.6 ± 0.2	
A4	BTMSE	1.05 ± 0.07	
A5	BTMSH	0.18 ± 0.05	
A6	BTMSH	0.41 ± 0.01	0.43 ± 0.01
A7	BTMSPA	0.22 ± 0.01	0.24 ± 0.01

[a] $k_{ac}{}^1$: Calculated from eq 28. [b] $k_{ac}{}^2$: Calculated from eq 26.

organosilica synthesis procedures, especially when prehydrolysis is used to control functional group homogeneity.

Experimental Section

Materials. TEOS, TMOS, MTMS, BTMSE, BTMSH, and BTMSPA (Figure 1) were purchased from Gelest at the highest purities available. Methanol (HPLC grade) and deionized ultrafiltered water were purchased from Fisher Scientific. Normalized 1.0 N HCl and 1.0 N NaOH were purchased from Alfa and dipropylamine (99+%) from Aldrich. All chemicals were used as received.

Sample Preparation. Before each kinetic experiment, two solutions were prepared. The first consisted of methanol and precursor; the second contained methanol, water, and HCl or NaOH. After setting up the spectrometer for the experiment, we mixed the two solutions in a polypropylene centrifuge tube very quickly and then injected mixed solution into the liquid transmission cell using a syringe. Series data were collected automatically at regular intervals after injection into the instrument. Time was recorded from the time of mixing the two stock solutions together.

Samples B1−B5 and B7 were made with the initial concentrations of 1.1 mol/L $SiOCH_3$ ($SiOCH_2CH_3$ in the case of TEOS), 1.1 mol/L H_2O, 23 mol/L CH_3OH, and 0.021 mol/L NaOH. The precursors used for these samples are listed in Table 1. The amount of water used for this series of samples is the stoichiometric amount required for complete hydrolysis. A quantity of dipropylamine equivalent to one amine per hexyl chain was added to sample B6 (prepared with BTMSH) for comparison with the effect of the integral amine in the chain of BTMSPA (sample B7). Sample B6 had a composition of 1.1 mol/L $SiOCH_3$, 1.1 mol/L H_2O, 22 mol/L methanol, 0.021 mol/L NaOH, and 0.18 mol/L dipropylamine.

Five samples were made in acidic conditions with the same composition. The precursors were TEOS, TMOS, MTMS, BTMSE, and BTMSH for samples A1−A5, respectively (see Table 2). The concentrations were 1.72, 0.28, 22, and 0.005 mol/L for $SiOCH_3$ ($SiOCH_2CH_3$), water, methanol, and HCl, respectively. A limited amount of water was chosen for this series to avoid the effects of first-shell substitution effects on reactivity.[25] Two samples, A6 and A7, were prepared specifically to compare the effect of an amine group present during the sol−gel reaction of BTMSH and BTMSPA. In the sample prepared with BTMSH (A6), a quantity of dipropylamine equivalent to the amount of amine in BTMSPA was added. The initial compositions of these two samples were 1.69 mol/L $SiOCH_3$, 1.69 mol/L H_2O, 21 mol/L methanol, 0.309 mol/L HCl, and x mol/L dipropylamine ($x = 0.282$ for A6, $x = 0$ for A7). An excess of HCl was added (above the moles of amine present) to ensure that the reaction proceeded under acidic conditions, even after complete titration of the amine.

Characterization. FTIR spectra were collected with a ThermoNicolet Nexus 470 Fourier transform infrared (FTIR) spectrometer with a DTGS detector. Kinetics were measured in situ in a demountable flow-through stainless steel transmission cell (Harrick Scientific) in which the liquid sample was introduced between two circular germanium windows. The temperature of the sample during the measurement was 21 ± 1 °C. Germanium was chosen because it is nonreactive and insoluble in water and alcohols. To avoid interference fringes in the FTIR spectra, we separated the germanium windows with two mismatched PTFE half-spacers that were 0.025 mm and 0.100 mm in thickness. The liquid sample between the windows thus formed a wedge. Spectra were collected at time intervals of 16.0 s for a total of 30 min. For each spectrum, 16 scans were averaged at a resolution of 4 cm^{-1} over the range 650−4000 cm^{-1}. Neat precursors and solvents were characterized by attenuated total reflection (ATR) FTIR with a 80 mm × 10 mm × 4 mm ZnSe internal reflection element mounted in a nickel-plated ATR trough (Pike Technologies).

Kinetic Model

Using the FTIR data (see below), we will be able to quantitatively monitor only functional group kinetics, specifically, the concentrations of water, ethanol, and alkoxide groups. Modeling of the sol−gel reaction thus is based on the evolution of these components. The assumptions used in the model will differ depending on the reaction conditions (acidic or basic). For both basic and acidic conditions, the relative importance of hydrolysis and condensation will be discussed in terms of three variables, defined as χ, r, and α. χ is the average degree of hydrolysis, defined as [SiOH]/([SiOH] + [SiOR]). r is the fractional conversion of alkoxides, defined as ($[SiOR]_0$ − [SiOR])/$[SiOR]_0$. α is the siloxane bond conversion, defined as 2[SiOSi]/$[SiOR]_0$. On the basis of the stoichiometry of eqs 1−4, we can derive expressions for χ and α from the two quantities that we will be able to independently measure at all times by FTIR (see below), the concentrations of water and alkoxide groups. The resulting expressions are

$$\chi = \frac{2w - r}{2w + 1 - 2r} \tag{5}$$

$$\alpha = 2(r - w) \tag{6}$$

where $w = ([H_2O]_0 - [H_2O])/[SiOR]_0$.

These overall parameters can be used to judge the relative rates of hydrolysis and condensation. If hydrolysis is the rate-limiting step, χ would be expected to be very small because [SiOH] is negligible. If $\chi = 0$, then from eq 5, $2w = r$, and from eq 6, r is expected to have a linear relationship with α with slope close to 1. On the other hand, if condensation is rate-limiting, then χ would be expected to be approximately constant. r would be expected to rapidly reach a relatively large value (equal to χ) and it would then have a linear relationship

with α. At this stage, the hydrolysis would remain almost at equilibrium because it is reversible and much faster than condensation.

Base-Catalyzed Methoxysilane Kinetics. The complete set of sol−gel reactions is depicted in eqs 1−4, but simplifying assumptions can be made to allow us to derive integrated kinetic equations. In basic conditions, hydrolysis has been shown to be the rate-limiting step with both TMOS[26] and TEOS.[26] Yoon et al. have demonstrated that water-producing condensation (eq 3) should be dominant over alcohol-producing condensation (eq 4).[68] Reverse condensation reactions can be neglected at the early stage of the reaction, so eq 3 adequately describes the condensation. Because condensation is much faster than hydrolysis, the re-esterification reaction (eq 2) can also be reasonably neglected. The functional group sol−gel reactions in basic conditions can therefore be simplified to just eqs 1 and 3. On the basis of these assumptions, the rate expressions in basic conditions are

$$d[\mathrm{SiOR}]/dt = -k_h[\mathrm{SiOR}][H_2O] \quad (7)$$

$$d[H_2O]/dt = -k_h[\mathrm{SiOR}][H_2O] + k_{cw}[\mathrm{SiOH}]^2 \quad (8)$$

$$d[\mathrm{SiOH}]/dt = k_h[\mathrm{SiOR}][\mathrm{H_2O}] - 2k_{cw}[\mathrm{SiOH}]^2 \quad (9)$$

Because the condensation rate is much higher than the hydrolysis rate, the concentration of SiOH can be treated as being at a pseudo-steady state.[25,28] With this assumption, we set eq 9 equal to zero. Integration of the differential equations yields the following expressions

$$[\mathrm{SiOCH_3}] = \frac{a}{1 - b\exp\left(-\frac{a}{2}k_h t\right)} \quad (10)$$

$$[H_2O] = \frac{a/2}{\frac{1}{b}\exp\left(\frac{a}{2}k_h t\right) - 1} \quad (11)$$

where $a = [\mathrm{SiOR}]_0 - 2[\mathrm{H_2O}]_0$ and $b = 2[\mathrm{H_2O}]_0/[\mathrm{SiOR}]_0$.

Absolute intensities of the bands for $SiOCH_3$ and H_2O can be measured from the FTIR spectra. The concentrations of $SiOCH_3$ and H_2O would be expected to follow Beer's law, but because the solution is a ternary H_2O/methanol/silane system, the extinction coefficients of $SiOCH_3$ and H_2O could be different than those in binary H_2O/methanol or silane/methanol mixtures. Moreover, the extinction coefficient of $SiOH_3$ may vary slightly for different silanes. To avoid the effect of differences in the extinction coefficient, eqs 10 and 11 can be re-expressed in terms of the absorbance measured at a particular reference time, t_r.

$$1 - \left(1 - b\exp\left(-\frac{a}{2}k_h t_r\right)\right)\frac{A(\mathrm{SiOCH_3})_r}{A(\mathrm{SiOCH_3})} = b\exp\left(-\frac{a}{2}k_h t\right) \quad (12)$$

$$1 + \left(\frac{1}{b}\exp\left(\frac{a}{2}k_h t_r\right) - 1\right)\frac{A(\mathrm{H_2O})_r}{A(\mathrm{H_2O})} = \frac{1}{b}\exp\left(\frac{a}{2}k_h t\right) \quad (13)$$

where $A(SiOCH_3)$ and $A(H_2O)$ are the absolute band intensities at any time t, and $A(SiOCH_3)_r$ and $A(H_2O)_r$ are the absolute intensities at the reference time t_r. The hydrolysis rate coefficient can be determined by nonlinear regression with either eq 12 or eq 13. Equation 12 has been shown[69] to give results consistent with detailed speciation modeling on the basis of the ^{29}Si NMR data of aminopropyltrimethoxysilane under basic conditions reported by Rousseau et al.[68]

Base-Catalyzed Ethoxysilane Kinetics in Methanol. In the above model, the precursor has the same alkoxy group as the alcoholic solvent. For the sol−gel reaction of TEOS in methanol, the transesterification of alkoxide groups (eq 14) also has to be considered. In addition, two different hydrolysis reactions can occur for ethoxides (eq 15) and methoxides (eq 16).

$$\mathrm{Si{-}OCH_2CH_3 + CH_3OH \xrightarrow{k_t} Si{-}OCH_3 + CH_3CH_2OH} \quad (14)$$

$$\mathrm{Si{-}OCH_2CH_3 + H_2O \xrightarrow{k_{he}} Si{-}OH + CH_3CH_2OH} \quad (15)$$

$$\mathrm{Si{-}OCH_3 + H_2O \xrightarrow{k_{hm}} Si{-}OH + CH_3OH} \quad (16)$$

Here, k_{hm} can be estimated independently from the hydrolysis kinetics of TMOS in methanol solution as described above.

If the transesterification reaction is competitive with the hydrolysis of TEOS, $SiOCH_3$ groups are expected to appear during the reaction. This makes it difficult to measure concentrations of both $SiOCH_3$ and $SiOCH_2CH_3$, because the band at 1196 cm^{-1} will overlap with the band at 1169 cm^{-1} (see below). However, ethanol evolves during transesterification, and its concentration can be used instead of $SiOCH_2CH_3$ to monitor the reaction.

With the assumption that $d[\mathrm{SiOH}]/dt \approx 0$, we obtain

$$\frac{d[\mathrm{SiOCH_2CH_3}]}{dt} = -k_t[\mathrm{SiOCH_2CH_3}][\mathrm{CH_3OH}] - k_{he}[\mathrm{SiOCH_2CH_3}][\mathrm{H_2O}] \quad (17)$$

$$\frac{d[\mathrm{CH_3CH_2OH}]}{dt} = k_t[\mathrm{SiOCH_2CH_3}][\mathrm{CH_3OH}] + k_{he}[\mathrm{SiOCH_2CH_3}][\mathrm{H_2O}] \quad (18)$$

$$-2\frac{d[\mathrm{H_2O}]/dt}{[\mathrm{H_2O}]} = k_{hm}[\mathrm{SiOCH_3}] + k_{he}[\mathrm{SiOCH_2CH_3}] \quad (19)$$

Because the initial solution does not contain ethanol, $[SiOCH_2CH_3] = [SiOCH_2CH_3]_0 - [CH_3CH_2OH]$. A large amount of methanol was used for the sample prepared with TEOS, so the concentration of methanol can be treated as a constant. We observed that the reaction rate of water was much smaller than the reaction rate of ethanol in our system. At the early stage of the reaction, the concentration of water remained nearly constant even though $d[H_2O]/dt$ was not zero. On the basis of these observations, we can assume that $[SiOCH_3] = [CH_3CH_2OH]$, $[CH_3OH] = [CH_3OH]_0$, and $[H_2O] = [H_2O]_0$ at the early stage of the reaction. Equation 19 can be rewritten as

$$-2\frac{d[\mathrm{H_2O}]/dt}{[\mathrm{H_2O}]} = (k_{hm} - k_{he})[\mathrm{CH_3CH_2OH}] + k_{he}[\mathrm{SiOCH_2CH_3}]_0 \quad (20)$$

Integration of eq 18 gives

$$1 - \frac{[\mathrm{CH_3CH_2OH}]}{[\mathrm{SiOCH_2CH_3}]_0} = \exp(-kt) \quad (21)$$

where $k = k_t[\mathrm{CH_3OH}]_0 + k_{he}[\mathrm{H_2O}]_0$.

The left side of eq 20 is equal to $-2(dA[\mathrm{H_2O}]/dt)/A[\mathrm{H_2O}]$, where $A[H_2O]$ is the absolute intensity of the peak for water. The extinction coefficient of water thus is not needed for eq 20. The extinction coefficient of CH_3CH_2OH is estimated from

the reference ethanol/methanol system. By fitting eq 20 to the water absorbance data, we can calculate k_{he}. For this purpose, the water vs time data are differentiated numerically. After obtaining k_{he}, we can calculate the value of k_t by fitting the concentration of ethanol with eq 21.

Acid-Catalyzed Kinetics. In contrast with the situation analyzed above, when the sol−gel reaction is carried out under acidic conditions, condensation is much slower than hydrolysis.[24] Initially, only hydrolysis occurs and the silanol concentration builds up rapidly before slowly decreasing. Condensation reversibility can be neglected in acidic conditions as well, but both water-producing and alcohol-producing condensation should be considered. The full set of reactions (eqs 1−4) gives the following kinetic expressions

$$d[\mathrm{SiOR}]/dt = -k_h[\mathrm{SiOR}][\mathrm{H_2O}] + k_h'[\mathrm{SiOH}][\mathrm{ROH}] - k_{ca}[\mathrm{SiOR}][\mathrm{SiOH}] \quad (22)$$

$$d[H_2O]/dt = -k_h[\mathrm{SiOR}][\mathrm{H_2O}] + k_h'[\mathrm{SiOH}][\mathrm{ROH}] + k_{cw}[\mathrm{SiOH}]^2 \quad (23)$$

$$d[\mathrm{SiOH}]/dt = k_h[\mathrm{SiOR}][\mathrm{H_2O}] - k_h'[\mathrm{SiOH}][\mathrm{ROH}] - 2k_{cw}[\mathrm{SiOH}]^2 - k_{ca}[\mathrm{SiOR}][\mathrm{SiOH}] \quad (24)$$

In a sol−gel reaction under acidic conditions, Rankin et al. found that the hydrolysis reaches quasiequilibrium when the water:SiOR molar ratio is large (≥ 1).[24] In this case, χ is a constant, so $[\mathrm{SiOH}] = \{\chi/(1-\chi)\}[\mathrm{SiOR}]$.[28] On the basis of these assumptions, one can derive eq 25

$$d[\mathrm{SiOR}]/dt = -2\chi\left(\frac{\chi k_{cw}}{1-\chi} + k_{ca}\right)[\mathrm{SiOR}]^2 \quad (25)$$

Integrating this equation gives

$$\frac{1}{[\mathrm{SiOR}]} - \frac{1}{[\mathrm{SiOR}]_q} = 2k_{ca}\chi\left(\frac{\chi k_{cw}/k_{ca}}{1-\chi} + 1\right)(t - t_q) \quad (26)$$

where $[\mathrm{SiOR}]_q$ is the concentration of SiOR at a specific time t_q after which quasequilibrium hydrolysis has been established.

The sol−gel reaction of TMOS in acidic conditions was studied by Assink et al.[24] k_{cw} was estimated to be 0.006 ± 0.001 L mol^{-1} min^{-1} and k_{ca} was estimated to be 0.0010 ± 0.0002 L mol^{-1} min^{-1}. The value of k_{cw}/k_{ca} is thus estimated to be around 6. Because most precursors used in this paper have the same $SiOCH_3$ groups, we assumed that this value is the same among these precursors. With this assumption, k_{ca} could be obtained by fitting eq 26 to the $[SiOCH_3]$ vs time data.

The concentration of water is needed to calculate the constant χ in eq 26. The extinction coefficient of water obtained from the binary water−methanol system was used for this estimation. When the water:SiOR ratio is very small (<1), χ will decrease during the sol−gel reaction in acidic conditions.[28] However, it is reasonable to assume that all water is consumed after fast hydrolysis and that all water produced by condensation will be immediately consumed by further hydrolysis.[28] The change in water concentration is negligible compared to the change in SiOR concentration, and eqs 22 and 23 can be combined to give

$$-d[\mathrm{SiOR}]/dt = k_{cw}[\mathrm{SiOH}]^2 + k_{ca}[\mathrm{SiOR}][\mathrm{SiOH}] \quad (27)$$

Because all water is consumed, $[\mathrm{SiOH}] = [\mathrm{SiOR}] - [\mathrm{SiOR}]_0 + 2[\mathrm{H_2O}]_0$. Substituting this expression in to eq 27 and integrating gives

$$\frac{([\mathrm{SiOR}] - a)([\mathrm{SiOR}]_c - ha)}{([\mathrm{SiOR}] - ha)([\mathrm{SiOR}]_c - a)} = \exp(-k_{ca}a(t - t_c)) \quad (28)$$

where $a = [\mathrm{SiOR}]_0 - 2[\mathrm{H_2O}]_0$, $h = k_{cw}/(k_{cw} + k_{ca})$, t_c is the time taken as the start of the condensation stage, and $[\mathrm{SiOR}]_c$ is the concentration of SiOR at t_c, which is $[\mathrm{SiOR}]_0 - [\mathrm{H_2O}]_0$. $h = 0.86$ was estimated by using the values of k_{ca} and k_{cw} reported by Assink et al.[70] for TMOS. The absolute intensity of SiOR at time t_c can be obtained from the FTIR spectra and used with the known initial concentrations of SiOR and H_2O to adjust the extinction coefficient for this band. This avoids the necessity of using the SiOR extinction coefficient obtained from a different system than the one being measured. For this reason, most samples studied here were prepared with small concentrations of water.

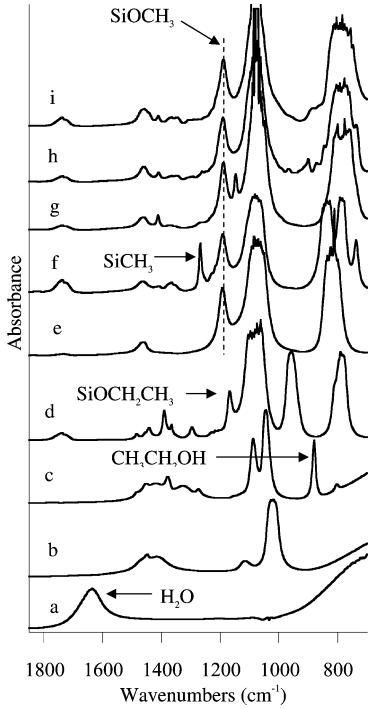

Figure 2. ATR-FTIR spectra of solvents and precursors: (a) water, (b) methanol, (c) ethanol, (d) TEOS, (e) TMOS, (f) MTMS, (g) BTMSE, (h) BTMSH, and (i) BTMSPA. Spectra were offset vertically to avoid overlapping.

Results and Discussion

FTIR Band Assignments. Spectra of the neat precursors and solvents were collected using FTIR spectroscopy of solutions in contact with a ZnSe ATR crystal. ATR provides a very short path length, which is useful for avoiding excessive adsorption with pure solvents and precursors. The angle of incidence of the IR beam was 45 degrees, and multiple reflections occurred along the 80 mm crystal.

Spectra of all solvents and precursors are compared in Figure 2. To quantitatively monitor the reaction, we must identify nonoverlapping bands associated with reacting species. Figure 2 shows that a well-separated band for water due to HOH bending[71] is available at 1657 cm^{-1}. No overlapping bands are observed in the other spectra. A band at approximately 1196 cm^{-1} is present in all methoxysilane precursors (attributed to $\rho(CH_3)$[71]) and is ideal to monitor the concentration of $SiOCH_3$

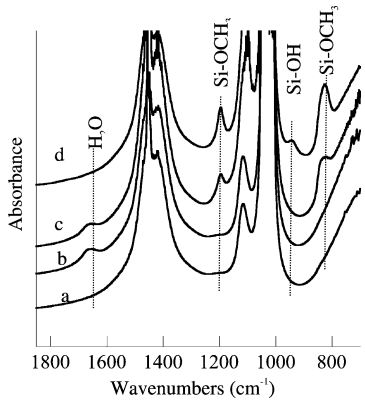

Figure 3. Transmission FTIR spectra of solvents and reacting solutions: (a) methanol; (b) water/methanol binary system ($[H_2O] = 1.24$ M); (c) TMOS/NaOH/H_2O/methanol (initial compositions: $[SiOCH_3] = 1.1$ M, $[NaOH] = 0.021$ M, $[H_2O] = 1.1$ M, and $[CH_3OH] = 23$ M) after 210 s; and (d) TMOS/HCl/H_2O/methanol (initial compositions: $[SiOCH_3] = 1.72$ M, $[HCl] = 0.005$ M, $[H_2O] = 0.28$ M, and $[CH_3OH] = 22$ M) after 210 s.

because it is sharp and clearly resolved from the other peaks associated with the methoxysilane precursors. Similarly, the ρ-(CH_3) band at 1169 cm^{-1}, present in the spectrum of TEOS, can be used to monitor the evolution of $SiOCH_2CH_3$.[71] This band, however, will overlap with the band of $SiOCH_3$ at 1196 cm^{-1} if both alkoxides coexist. Another strong band at 961 cm^{-1} is also associated with $SiOCH_2CH_3$, but this band will not be used to monitor $SiOCH_2CH_3$ because it will overlap with the growing Si−OH peak (see below). The evolution of $SiOCH_2$-CH_3, however, can be indirectly monitored by the 881 cm^{-1} C−C/C−O stretching band of ethanol.[72]

Because it is a noninvasive technique, ATR-FTIR with a ZnSe crystal is a common technique for monitoring reaction kinetics. The short path length provided by the ATR method is useful for solutions containing a significant concentration of water. However, the ZnSe crystal is not sufficiently robust under strongly basic or acidic conditions for our investigation. In the rest of this paper, we will report transmission data collected in a stainless steel liquid cell with Ge windows and mismatched PTFE spacers.

Figure 3 illustrates the bands associated with intermediates in mixed, reacting systems. Trace a is the spectrum of pure methanol. Trace b is a solution of water in methanol. Trace c is a mixed water/methanol/NaOH/TMOS solution at 210 s after mixing. Trace d is a mixed water/methanol/HCl/TMOS solution at 210 s after mixing. The band at around 1657 cm^{-1} in trace b appears at the same position as the band in the spectrum of pure water, and will be used to quantify the amount of water present. The bands at 1196 and 833 cm^{-1} in trace c are from Si−OCH_3. Because it is more clearly resolved, the band at 1196 cm^{-1} is used to monitor the evolution of Si−OCH_3. Both methanol and TMOS have strong bands in the regions at around 1112 cm^{-1} to 1025 cm^{-1}. The stretching bands of Si−O−Si are also found in this region. The relative intensities of the bands in this region have been used to trace the appearance of linear and cyclic Si−O−Si species before.[71,73] However, these bands cannot be used to quantitatively monitor the kinetics of the sol−gel reactions because they overlap strongly and are saturated because of the large path length of the transmission cell. A band at ~948 cm^{-1} is observed in trace d but not in trace *c*. Because silanols are present in large quantities in acidic but not basic sol−gel solutions, this band is associated with Si−O stretching of SiOH groups.[65,74]

Below, we will also discuss some of the qualitative features that evolve during the polycondensation of the silanes under investigation. However, following the assignments made here, we will use the integrated intensities of bands at 1657, 1196, and 881to quantify the evolutions of H_2O, $SiOCH_3$, and CH_3-CH_2OH, respectively.

Quantitative Interpretation of FTIR data. FTIR has been successfully used to monitor the evolution of Si−OCH_3 during a sol−gel reaction before.[1,29,60] In addition, we used the intensities of water and ethanol bands to follow the reactions of our series of precursors. As expected according to Beer's law, linear relationships between the absorbances and concentrations of $SiOCH_3$ from TMOS, H_2O, and CH_3CH_2OH in methanol were obtained (see the Supporting Information, Figure SI-1). The background from methanol was flat near 1169 cm^{-1}, so absolute absorbances of $SiOCH_3$ were obtained by simply integrating the peak area. Because the baseline of methanol is somewhat curved near 1657 and 881 cm^{-1}, absolute absorbencies for H_2O and CH_3CH_2OH were obtained after subtracting the methanol background spectrum. In all cases, a good linear relationship is found by regression for $SiOCH_3$, H_2O, and CH_3-CH_2OH in methanol.

Whereas we have shown here that Beer's law is obeyed for nonreacting mixtures, the extinction coefficient of species in reacting sol−gel solutions may differ slightly from those in the reference silane/methanol and water/methanol systems. We designed our modeling equations so that they are as insensitive as possible to the precise values of extinction coefficients (see above). It is only necessary that a linear relationship between concentration and absorbance be maintained for a short reaction time.

Comparison of Hydrolysis Kinetics in Basic Conditions. The hydrolysis kinetics of silanes with different alkoxide groups have been compared before.[60,61,63] A bulky alkoxide group leads to slow hydrolysis. The effects of the size of non-hydrolyzable organic groups was also compared among silanes with different organic groups.[1,60] A bulky organic such as a long alkyl chain decreases the rate of hydrolysis. These effects are observed because hydrolysis in basic conditions is a nucleophilic substitution reaction.[75] A large group attached to silicon causes steric crowding in the transition states, which inhibits the nucleophilic reaction. However, no study has been carried out on the differences in sol−gel reaction kinetics between nonbridged organotrialkoxysilanes and their corresponding bridged silanes. Moreover, effects of the length and type of the bridging chains on the hydrolysis have not been reported. In this section, we investigate effects of alkoxy groups and bridging chains on hydrolysis kinetics in basic conditions.

For all samples in basic conditions (B1−B7), no silanol band could be observed. This confirms the validity of the SiOH pseudo-steady-state assumption used to model these systems. For the methoxysilane samples (B2−B7), intensities of both $SiOCH_3$ and H_2O decrease monotonically during the reaction. The evolution of selected spectra of sample B2 is shown in Figure 4. The evolutions of the spectra of the other samples are shown in the Supporting Information (Figures SI-2−SI-5). Both $SiOCH_3$ peaks at 1196 and 831 cm^{-1} decrease in intensity with time. A weak shoulder of the peak at 1196 cm^{-1} appears after several minutes of reaction and then increases in intensity. Lenza and Vasconcelos deconvoluted the Si−O−(Si) stretching bands of hydrolyzed TEOS into five peaks at around 1040, 1080, 1100, 1160, and 1200 cm^{-1}.[75] Of these, the peaks at 1080 and 1200 cm^{-1} were attributed to cyclic structures and the others to linear structures.[71,75] The presence of the shoulder at 1216 cm^{-1} in

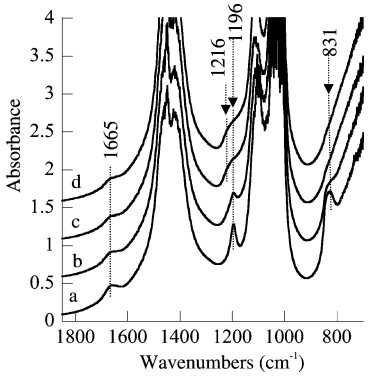

Figure 4. FTIR spectra of B2 (TMOS) at different times after mixing: (a) 60, (b) 380, (c) 1180, and (d) 1820 s; offset vertically by 0.5, 1.0, and 1.5 for b, c, and d, respectively.

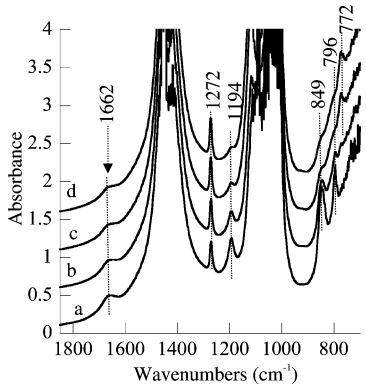

Figure 5. FTIR spectra of B3 (MTMS) at different times after mixing: (a) 60, (b) 380, (c) 1180, and (d) 1820 s; offset vertically by 0.5, 1.0, and 1.5 for b, c, and d, respectively.

our spectra might indicate the production of cyclic Si−O−Si species, although the band is too weak to allow a quantitative measure.[76] The qualitative features of the evolving spectra for samples B5−B7 are similar to those of sample B2. The bands associated with $SiOCH_3$ and H_2O decrease with time, and a weak shoulder appears during the reaction near the $SiOCH_3$ peak at 1196 cm^{-1}.

The evolution of the spectra for samples B3 (Figure 5) and B4 (See the Supporting Information, Figure SI-5) differs from that of sample B2. For pure MTMS (Figure 2), two peaks associated with the attached methyl group are identified at 1265 and 738 cm^{-1} and have been assigned to CH_3 symmetric deformation and Si−C stretching from Si−CH_3, respectively.[77] Three additional peaks from the precursor are identified at 1194, 833, and 784 cm^{-1}. The peak at 738 cm^{-1} shown in Figure 2 for MTMS is not apparent in the reacting system, possibly because of its low intensity in the mixture. As the reaction proceeds, intensities of both $SiOCH_3$ bands decrease. During the reaction, a band appears at 772 cm^{-1} and becomes stronger. At the same time, the intensity of the peak at 1272 cm^{-1} also increases. Unlike samples B2 and B5−B7, no weak shoulder appears near the 1194 cm^{-1} band for sample B3. The peaks at 1272 and 772 cm^{-1} are the only peaks that became stronger during the reaction, which suggests that the increase in their intensity is due to the formation of condensed species containing Si−O−Si bonds. The band at 772 cm^{-1} may be associated with C−Si−O asymmetric stretching.[78] The increase in intensity at 1272 cm^{-1} may be associated with the formation of a strained siloxane ring; for instance, hexamethylcyclotrisiloxane has a band in a similar location, whereas other linear and cyclic siloxanes do not.[79]

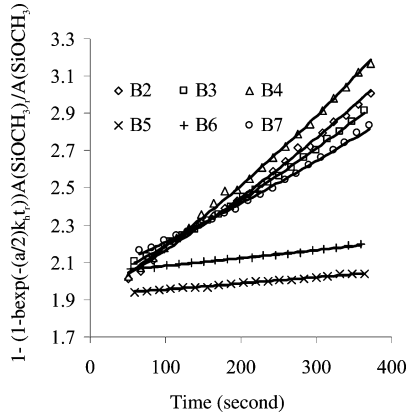

Figure 6. Fits of experimental data derived from the concentration of $SiOCH_3$ with eq 12.

A similar trend is observed during the reaction of sample B4 (see the Supporting Information). A weak peak appears at 1272 cm^{-1} and increases in intensity during the reaction. Also, no weak shoulder is present near the $SiOCH_3$ band at 1196 cm^{-1}. However, unlike sample B3, a peak does not appear near 772 cm^{-1}. Because sample B4 contains no methyl groups (it is made with BTMSE), the increasing band at 1272 cm^{-1} must be caused by a particular Si−O−Si structure, such as the seven-atom bicyclic dimer identified by Loy and co-workers during bis-(triethoxysilyl)ethane polymerization.[1] It is also possible that the condensed species in B3 and B4 are similar to those found in B2 and B5−B7, but that the frequencies associated with the structures are much different.

Prior to applying our model to the base-catalyzed methoxysilane samples, we prepared $r-\alpha$ plots for samples B2−B7 (see the Supporting Information, Figure SI-6). The slope of all $r-\alpha$ plots is close to 1, which is consistent with the assumption that hydrolysis is the rate-limiting step. Hydrolysis rate coefficients were calculated by nonlinear regression using the data collected during the first 360 s of reaction for all samples. Fits of eq 12 to the experimental data for all basic compositions are shown in Figure 6. Similar fits to the water intensity data were found using eq 13 (see the Supporting Information, Figure SI-7). Excellent fits were obtained in all cases, and the hydrolysis coefficients found on the basis of the evolution of the $SiOCH_3$ data (k_{h1}) and the H_2O data (k_{h2}) are summarized in Table 1 (the uncertainties are 95% confidence intervals obtained during the fitting).

The evolution of the concentration of $SiOCH_3$ in each sample over a longer interval (1800 s) was calculated with eq 10 using the values of k_{h1} in Table 1. Figure 7 shows a comparison of the experimental data with these calculated curves (curves for the evolution of water are shown in the Supporting Information but show similar trends). The calculated data are more consistent with the experimental data over the entire time interval for samples B3, B5, and B6. This indicates that the model describes the sol−gel reaction better for these three samples than for B2, B4, and B7. Experimental data of B2, B4, and B7 level off after 1000 s. This might be due to hydrolysis reversibility becoming important late in the reaction,[80] but this is unlikely because the concentration of SiOH groups does not increase to measurable levels in the FTIR spectra. Therefore, the most likely explanation for the trends in Figure 7 is that hydrolysis reactivity changes as the reaction proceeds. For all cases where a mismatch is observed, there is an average of at most one OCH_3 group remaining per silicon site. The presence of three stable, bulky ligands (siloxane or organic) could significantly decrease the rate of the reaction compared to other silicon sites. This effect

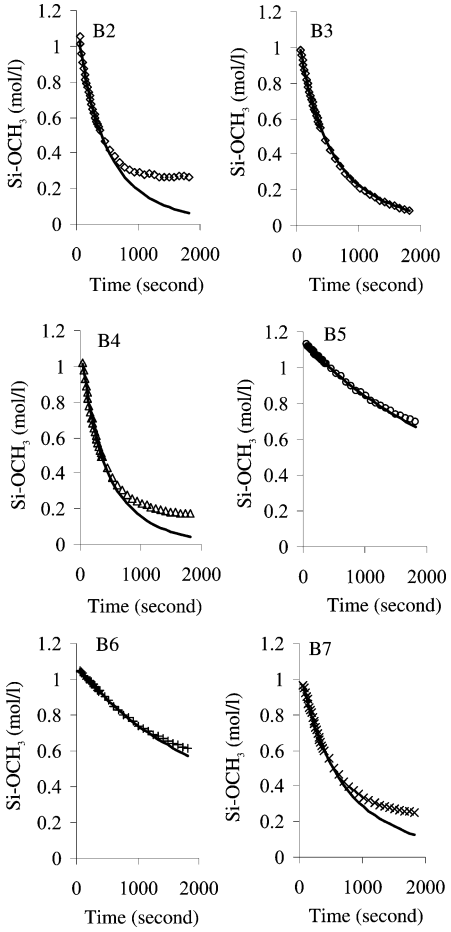

Figure 7. Comparisons of the experimental data (scattered points) and the calculated curves (continuous curves) for $SiOCH_3$.

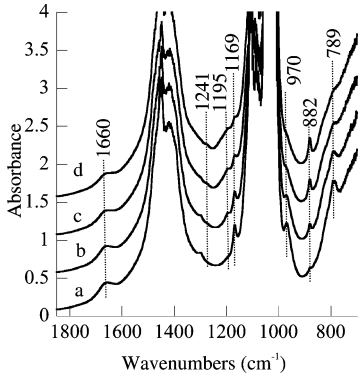

Figure 8. FTIR spectra of B1 (TEOS) at different times after mixing: (a) 60, (b) 380, (c) 1180, and (d) 1820 s; offset vertically by 0.5, 1.0, and 1.5 for b, c, and d, respectively.

is not observed in the MTMS sample (B3), but this could be because the methyl group is so small. The consistency of experimental data and calculations for samples B5 and B6 is simply because the hydrolysis is so much slower with BTMSH. The reaction does not progress enough that the change in hydrolysis reactivity becomes important. To avoid difficulties in interpreting the effects of changing reactivity, we have chosen the experimental data in the first 360 s to estimate the hydrolysis coefficient, as described above.

For TEOS, the analysis is complicated by the possibility of transesterification. The evolution of the water band (~1650 cm^{-1}) in sample B1 (Figure 8) is similar to the evolution of the band in the methoxysilane samples. Also, consistent with the

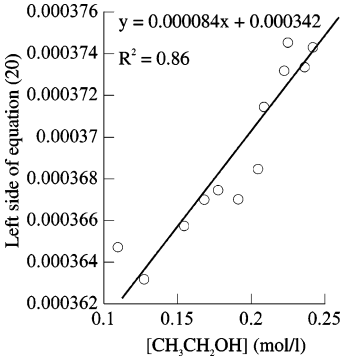

Figure 9. Fitting of the experimental data for sample B1 with eq 20.

fact that TEOS is the precursor, no $SiOCH_3$ band is observed initially. Peaks at 1298, 1169, 970, and 789 cm^{-1} are associated with TEOS. As the reaction proceeds, a weak band from $SiOCH_3$ appears at 1195 cm^{-1}. The intensity of this peak passes through a maximum. A band associated with CH_3CH_2OH (~882 cm^{-1}) grows as the reaction proceeds. The evolution of the spectra is consistent with the reactions expected for TEOS in methanol. The appearance of $SiOCH_3$ is due to transesterification. $SiOCH_2CH_3$ and $SiOCH_3$ are simultaneously consumed because of hydrolysis and subsequent condensation reactions. Ethanol is produced by both the transesterification and hydrolysis of $SiOCH_2CH_3$. Because the bands of $SiOCH_2CH_3$ at 1169 cm^{-1} and $SiOCH_3$ at 1195 cm^{-1} overlap, the kinetics is modeled on the basis of the more easily resolved peak from ethanol at 881 cm^{-1}. The concentration of water remains approximately constant during the early stage of the reaction (see the Supporting Information, Figure SI-9). This verifies the assumption used to model the reactions of TEOS. Equation 20 was applied to the water and ethanol concentration data to provide the fit shown in Figure 9. The hydrolysis coefficient found is $(2.93 \pm 0.04) \times 10^{-4}$ M^{-1} s^{-1}. An exponential fit using eq 21 and the ethanol concentration data yielded an estimate of the transesterification coefficient of $(0.38 \pm 0.05) \times 10^{-4}$ $M^{-1}s^{-1}$. Although the rate coefficient for hydrolysis is greater, transesterification plays a significant role in sample B1 because of the concentration of methanol is large (22 M).

The hydrolysis coefficients summarized in Table 1 reveal the kinetic trends induced by gradually changing the structure of the silane. The trends in the hydrolysis coefficients calculated from the $SiOCH_3$ band (k_{h1}) and the H_2O band (k_{h2}) are consistent for all samples. The first thing that we notice is that the hydrolysis coefficient of TEOS is much smaller than that of TMOS. This is consistent with the steric effect induced by the bulkier ethoxy ligand. Moving down the table, we find that the hydrolysis of MTMS is only slightly slower than that of TMOS. The substitution of a methoxy group with a methyl group would not be expected to induce a change in the steric bulk near the reaction center. However, a methyl group would be expected to be more electron-donating than a methoxy group, which should increase the electron density at the silicon, which in turn slows down the hydrolysis under basic conditions.[81] This is as expected.

The newest results reported in Table 1 are the effects of bridging. BTMSE is the bridged silane corresponding to MTMS. It has two $Si(OCH_3)_3$ groups connected with a short ethylene chain. The organic group attached to each silicon in BTMSE is bulkier than it is in MTMS, but the bridging chain is so short that it is possible that the electron density of the silicon in BTMSE decreases because of electron withdrawal by the silicon at the other end of the molecule. The methoxy groups at the

opposite end from the reacting site may also be better solvated than the methyl group of MTMS, which would be expected to accelerate hydrolysis. Okumoto et al. showed that solvation of alkoxysilanes by water clusters may significantly enhance their reactivity.[82] The net effect is that hydrolysis rate of BTMSE increases somewhat compared to MTMS. In contrast, for BTMSH, the bridging chain is too long for the two $Si(OCH_3)_3$ groups to interact with each other. The electron density of the silicon increases, as we would expect for a long alkyl group attached to silicon. At the same time, BTMSH is much bulkier than BTMSE. The length of the alkyl chain would also prevent any favorable solvation effects because of the proximity of methoxy groups from the opposite end of the chain. All of these factors favor a decrease in the hydrolysis rate, and a large decrease is, in fact, observed.

The next change in the silanes is in going from BTMSH (B5) to BTMSPA (B7). The introduction of the amine into the hexylene bridge causes a large increase in the hydrolysis rate of the precursor. Because an amine can affect the pH of the solution or could act as a specific catalyst for the sol−gel reaction,[83] we measured the hydrolysis kinetics of sample B6, in which BTMSH was the precursor and a concentration of dipropylamine was added equivalent to that in sample B7. As Table 1 shows, the hydrolysis rate increases only slightly because of the addition of the amine. Therefore, we can rule out any intermolecular catalytic effect associated with having amines in the solution. Alkylamines are known to be electron donors.[81] The amine group in BTMSPA may donate electrons to the silicon even through three C−C bonds. This should lead to lower reactivity for BTMSPA, but in fact, we observe an increase in the hydrolysis rate. BTMSPA and BTMSH should be equally bulky near the hydrolysis reaction site, so we cannot attribute the increase in the hydrolysis rate to either steric effect or electronic induction effects. The best explanation for the increase in the hydrolysis rate of BTMSPA may be that electrostatic and hydrogen bonding between the amines in the bridging chain and water or methanol lead to local solvent clustering which increases the hydrolysis rate.[60]

From the investigation of silane hydrolysis in basic conditions, we see that the reactivity of a silane can be explained primarily by the inductive and steric factors of its constituents, even for bridged silanes. As is well-known,[81] both steric and inductive factors are very important for the sol−gel reaction under basic conditions. Both a high electron density at silicon and bulky groups near a silicon site slow the reaction. Thus, TEOS is hydrolyzed more slowly than TMOS. The substitution of a methoxy group with a methyl group decreases the hydrolysis rate slightly. When the bridging chain is as short as an ethylene, the two $Si(OCH_3)_3$ groups interact with each other and the inductive factor is dominant over the steric factor. Thus, the hydrolysis rate increases. In addition, ab initio calculations have suggested that solvent cluster association with the reacting molecule may play a significant role in promoting sol−gel reactions.[25,28] Solvation of the methoxy groups at the opposite end from the reaction site may contribute to the fast hydrolysis of BTMSE. When the bridging chain is as long as a hexylene, the steric factor is dominant over inductive and solvation effects, and the bridging organic retards the reaction rate. The presence of an amine group in the bridging chain increases the reaction rate, but not because of catalytic or electron inductive effects. The best explanation for this is that the amine induces local solvent clustering near the silicon site, which enhances the hydrolysis rate.

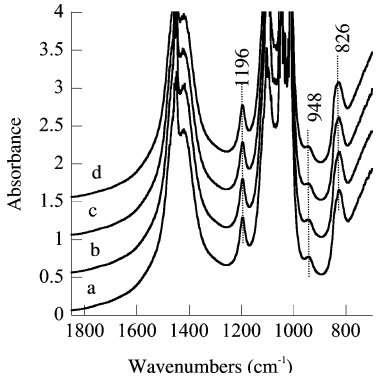

Figure 10. FTIR spectra of A2 (TMOS) at different times after mixing: (a) 60, (b) 380, (c) 1180, and (d) 1820 s; offset vertically by 0.5, 1.0, and 1.5 for b, c, and d, respectively.

Comparison of the Kinetics of Condensation in Acidic Conditions. In acidic conditions, hydrolysis is much faster than condensation,[1,60] and the sol−gel reaction rate is limited by the latter reaction. Condensation in acidic conditions is a nucleophilic substitution reaction, so it is expected to be influenced by both steric and inductive factors.[1] Condensation should be more sensitive to steric factors than hydrolysis because two silicon sites participate in the reaction (rather than one silicon site and water). The inductive effect depends on the pH value of the solution. If the reaction occurs below the isoelectric pH of the silicon site, a positively charged intermediate will be involved, and a decrease in the acidity will accelerate the condensation rate.[1] On the other hand, above the isoelectric pH of the silicon site, a decrease in acidity will decelerate condensation.[1] The isoelectric point of highly condensed silica (colloidal silica) is near pH 2,[84] but for monomeric silicic acid, the pK_a value reported by Iler suggests an isoelectric pH closer to 4.[85] This makes sense, because siloxane groups are more electron-withdrawing than hydroxyl groups. The isoelectric pH of organoalkoxysilanes would be expected to be shifted even higher; for instance, that of γ-glycidoxypropylsilanetriol is 4.5.[71,75] Thus, we expect all of our acid-containing samples to follow an acid-catalyzed condensation mechanism.

Representative FTIR spectra of sample A2 are shown in Figure 10 and illustrate the changes typically observed in the acid-catalyzed methoxysilane samples. Spectra of other samples are shown in the Supporting Information. The Si−OCH_3 band (1196 cm^{-1}) remains clearly resolved during the reaction for all samples and its intensity decreases with time. No shoulder due to condensed species interferes with this peak, and we expect to have a linear relationship of the intensity of this band with the $SiOCH_3$ concentration throughout all experiments. For all samples, a peak appears at around 950 cm^{-1} (948 cm^{-1} for sample A2) that can be assigned to the stretching vibration of Si−OH.[75] The intensity of this peak decreases over time in all samples. The presence of this peak and the absence of a water band in the spectra suggests that the hydrolysis is much faster than condensation, as we proposed in our model. A small peak appears at 900 cm^{-1} only for sample A5. This peak can be attributed to nonbridging free $Si-O^-$ bonds.[75] Like the samples prepared in basic conditions, peaks associated with condensed species are identified at 1270 and 771 cm^{-1} in sample A3 and at 1270 cm^{-1} in sample A4.

Plots of r vs α (see the Supporting Information, Figure SI-13) for all acidic-catalyzed samples yielded straight lines with slopes of ~2. This confirms that condensation is rate-limiting after the initial hydrolysis, as discussed above. We also confirmed the assumed linear relationship between [$SiOCH_3$]

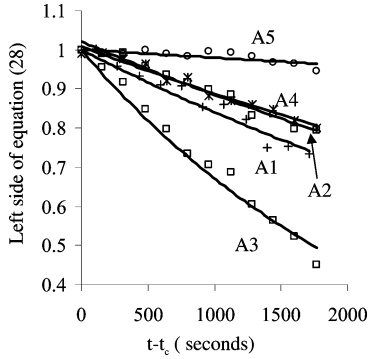

Figure 11. Fits of experimental data with eq 28 for samples A2 to A5.

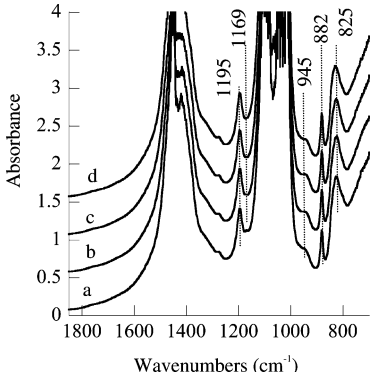

Figure 12. FTIR spectra of A1 (TEOS) at different times after mixing: (a) 60, (b) 380, (c) 1180, and (d) 1820 s; offset vertically by 0.5, 1.0, and 1.5 for b, c, and d, respectively.

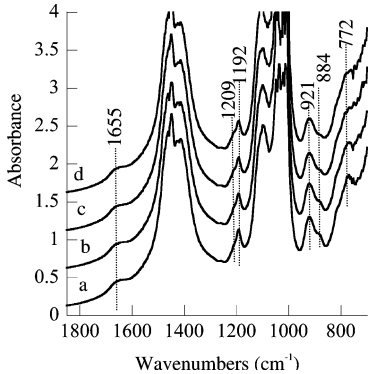

Figure 13. FTIR spectra of A7 (BTMSPA) at different times after mixing: (a) 60, (b) 380, (c) 1180, and (d) 1820 s; Offset vertically by 0.5, 1.0, and 1.5 for b, c, and d, respectively.

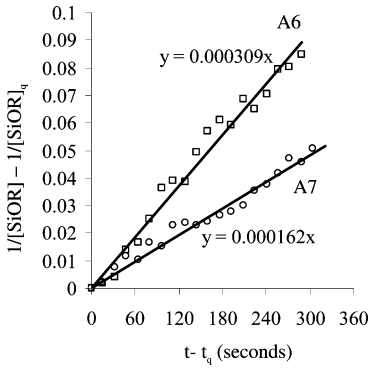

Figure 14. Fits of experimental data with eq 26 for sample A6 and A7.

and the intensity of the SiOH peak for all samples in this series (see the Supporting Information). The condensation coefficient k_{ac} was estimated by fitting the experimental data in the first 1800 s with eq 28. The fitted plots are shown in Figure 11. All of the experimental data could be fit very well, which suggests that the assumptions made in the model are reasonable.

The evolution of spectra for the sample A1 is shown in Figure 12. A weak peak from $SiOCH_2CH_3$ at around 1169 cm^{-1} is barely visible at around 55 s, but this peak is not observed after 100 seconds of the reaction. The other band associated with $SiOCH_2CH_3$, at 789 cm^{-1}, also disappears within 100 seconds. Consistent with the loss of ethoxy groups in TEOS, a peak for CH_3CH_2OH is observed at 882 cm^{-1} whose intensity remains nearly constant during the entire time interval monitored. The peak for $SiOCH_3$ is very strong after 55 s of reaction, and its intensity decreases slowly with time after that. No peak for water is observed after 55 s. Similar to the other acid-catalyzed samples, a SiOH peak at 948 cm^{-1} appears after 55 s and slowly decays. All of these trends suggest that the transesterification and the hydrolysis occur very quickly, much faster than the condensation. Within 100 seconds, almost all $SiOCH_2CH_3$ groups are consumed by hydrolysis and transesterification. The state of this system after 100 s actually is similar to the reaction system with TMOS as the precursor except that a small amount of ethanol was present in the solvent. By fitting the experimental data using eq 28, we obtain k_{ca} of $SiOCH_3$ with the presence of a small amount of ethanol. k_{ca} is $(1.4 \pm 0.1) \times 10^{-4}$ M^{-1} S^{-1}, which is close the value measured with TMOS (Table 2). This is consistent with the expectation that the condensation of TEOS in methanol solution is similar to the condensation of TMOS in the same system.

A larger ratio of H_2O:$SiOCH_3$ (1:1 molar ratio) was used for samples A6 and A7. Peaks from Si−OCH_3, H_2O, and Si−OH are identified in the spectra of A6 (see the Supporting Information). A small peak appears at 876 cm^{-1} that is attributed to the to nonbridging free Si−O$^-$ bonds.[75] Peaks from $SiOCH_3$ are identified at 1192 and 772 cm^{-1} in the spectra of sample A7 (Figure 13). The small shoulder of the 1192 cm^{-1} peak is attributed to condensed cyclic Si−O−Si species.[60] This peak becomes stronger during the reaction. Similar to sample A6, a small peak (884 cm^{-1}) from nonbridging free Si−O$^-$ bonds appears at the shoulder of the major peak (921 cm^{-1}). Similar to the case in the base-catalyzed hydrolysis, the small peak at 1209 cm^{-1} makes it difficult to integrate the absolute intensity of the $SiOCH_3$ band at 1192 cm^{-1}. Data collected at a very early stage of the sol−gel reaction thus have to be used to avoid the interference of the condensed Si−O−Si species by assuming the contribution from these species is negligible in that period. Data collected within first 300 s were used for fitting of samples A6 and A7. χ is almost constant over this interval for both samples (see the Supporting Information), as expected for hydrolysis quasiequilibrium. Equation 26 thus can be used as the model for the two samples. The extinction coefficients calculated from the corresponding basic systems were used to estimate the concentration of $SiOCH_3$. The extinction coefficient of water was estimated from the concentration of H_2O at the start of the quasiequilibrium of the hydrolysis. At the start of the quasiequilibrium state, $[H_2O]_q \approx [H_2O]_0 - [SiOCH_3]_0 + [SiOCH_3]$ by assuming the condensation in the fast hydrolysis step was negligible. With these assumptions, good fits to the experimental data are obtained using eq 26, as shown in Figure 14.

The concentration of water remains almost constant with time for samples A6 and A7, so it is also possible to determine the condensation coefficients using the alternative condensation model discussed above (eq 28). The water concentrations and

fits are shown in the Supporting Information. For A6, the water concentration is constant and the models give similar condensation rate coefficients. The water concentration in A7 decreases slightly with time. The assumption of constant water concentration has caused a small difference between the condensation coefficients calculated by the two models. The coefficient calculated from eq 26 is expected to be more reliable.

k_{ac} values for all acidic samples are compared in Table 2. The pH value calculated from the acid concentration (assuming ideal mixing) for samples A2−A5 is around 2.3, and for samples A6 and A7, the calculated pH value (assuming that all amine groups were titrated by the acid) is 1.6. The pH values of A6 and A7 solutions measured with a combination glass electrode were ∼1.4, but the response time was so slow that it took ∼15 min to get a stable reading. This value may be low because of the activity and junction potential effects.[86,87] To confirm that the pH values are consistent with expectations, the pH values of the stock solutions used to prepare A6 and A7 were measured with the same electrode. With δ corrections from the literature,[88] the pH was measured to be 1.5 (vs 1.3 expected) for the A6 stock solution (3.38 mol/L H_2O, 0.618 mol/L HCl, and 0.564 mol/L dipropylamine in methanol) and 0.16 (vs 0.21 expected) for the A7 stock solution (3.38 mol/L H_2O and 0.618 mol/L HCl in methanol). The slight disagreement might be due to nonideal solution effects not accounted for by δ, but show that the pH values are close to expectations. At these pH values, all monomers should react by an acid-catalyzed mechanism. The condensation rate coefficient of TEOS cannot be directly measured because of fast transesterification, but the results after transesterification agree with those of TMOS. Comparing A2 and A3, we find that the condensation rate of TMOS is slower than that of MTMS. The difference between TMOS and MTMS may be partially due to the inductive effect of replacing a methoxy group with a methyl group. Because the methyl group is more electron-donating, the silanol acidity should be reduced for MTMS. Under acid catalysis, this should increase the condensation rate. When BTMSE is used instead of MTMS, the electron density of Si is expected to decrease, as discussed in the basic situation. This increases the silanol acidity thus decreasing the condensation rate. The increased steric bulk of BTMSE also should decrease condensation reactivity. The distance between the two silicon ends in BTMSH is much longer than that in BTMSE. The inductive effect from the $SiOCH_3$ at the other end will be negligible. BTMSH is much bulkier than BTMSE, which retards condensation significantly, as observed (sample A5). Different reaction conditions have been used for samples A5 and A6. The condensation in sample A6 is faster than that in sample A5 because of the lower pH and the catalytic effect of the amine in A6. For BTMSPA, the silanol acidity is expected to decrease slightly because of the electron-donating properties of the amine group. This should increase the condensation rate at pH < 2. Moreover, the bridging chain in BTSMPA is slightly longer than that in BTMSH, which may also reduce the condensation rate. However, because there are three C−C bonds between the amine and the silicon in BTMSPA, the inductive effect from the amine should be small. Also, under acidic conditions, both amines and silanols may be positively charged, so there should be no enhancement in rate due to localized clustering of silane reactants. These expectations are consistent with the small difference between condensation rates of A6 and A7 as shown in Table 2.

To summarize for the acid-catalyzed series, consistent with known trends,[81] steric factors have been found to always strongly affect the kinetics of the condensation in acidic conditions. An inductive effect may influence the condensation rate for MTMS compared to TMOS, but otherwise, the results are dominated by steric effects.

Conclusions

Six silanes have been selected to investigate effects of gradual changes in organic substitution and bridging on sol−gel reaction kinetics in basic and acidic conditions. The differences in kinetics can mostly be explained by the differences in steric and inductive effects expected for different organic substituents. The primary effect of alkoxide group replacement is steric: $SiOCH_2CH_3$ is bulkier than $SiOCH_3$. The substitution of a methoxy group in TMOS with a methyl group (to create MTMS) increases the electron density of the silicon but is expected to have little effect on how crowded the silicon site is. The two $Si(OCH_3)_3$ ends of the short bridged silane BTMSE interact with each other, resulting in a slight decrease in electron density at silicon for both ends. The proximity of the methoxy groups from one end may also enhance the solvation in the vicinity of the reactive end of BTMSE. These effects are absent with a longer bridging group, and the organic bridge of BTMSH is much bulkier than BTMSE, which retards both hydrolysis and condensation significantly. The main difference between BTMSH and BTMSPA is the amine group contained in BTMSPA, which should be mildly electron-donating toward silicon. Most of the kinetic trends can be explained by these changes. In basic conditions, hydrolysis is rate-determining, and the rate decreases as the electron density at silicon increases or as steric bulk increases. In acidic conditions, condensation is rate-limiting, and steric factors are very influential. Inductive effects depend on the pH: if the reaction is still base-catalyzed, a higher electron density at silicon decreases the rate, whereas if it is acid-catalyzed, this will increase the condensation rate.

Exceptions to the steric and inductive trends were found for BTMSPA. In basic conditions, the hydrolysis rate of BTMSPA increased compared to BTMSH, which is inconsistent with both the slightly larger steric bulk of the chain and the electron-donating nature of the amine. However, a reason for acceleration may be localized clustering of water (and possibly methanol) with the amine in the chain, which can lower the activation energy for hydrolysis. In acidic conditions, the electron-donating effect of the amine is not observed to increase the hydrolysis rate, but this is consistent with the steric effect of introducing the amine and the absence of favorable interactions between protonated amines and silanols or water at this pH.

Acknowledgment. This report is based on work supported by the National Science Foundation under CAREER Grant CTS-0348234. B.T. acknowledges partial support through a Kentucky Research Challenge Trust Fund Fellowship. We thank Xin Li for performing the pH measurements.

Supporting Information Available: Calibration curves; FTIR spectra of samples A3−A6 and B2−B7; r−α plots of samples A2−A5 and B2−B7; exponential fits of eqs 13 and 28; comparison of calculated and experimental concentrations of H_2O; plots of [$SiOCH_3$] vs A[SiOH]; plot of χ vs time; plots of changing H_2O concentration. This material is available free of charge via the Internet at http://pubs.acs.org.

References and Notes

(1) Brinker, C. J.; Scherer, G. W. *Sol−Gel Science*; Academic Press: San Diego, 1990.

(2) Beck, J. S.; Vartuli, J. C.; Roth, W. J.; Leonowicz, M. E.; Kresge, C. T.; Schmitt, K. D.; Chu, C. T.-W.; Olson, D. H.; Sheppard, E. W.; McCullen, S. B.; Higgins, J. B.; Schlenker, J. L. *J. Am. Chem. Soc.* **1992**, *114*, 10834.
(3) Kresge, C. T.; Leonowicz, M. E.; Roth, W. J.; Vartuli, J. C.; Beck, J. S. *Nature (London)* **1992**, *359*, 710.
(4) Monnier, A.; Schüth, F.; Huo, Q.; Kumar, D.; Margolese, D.; Maxwell, R. S.; Stucky, G. D.; Krishnamurty, M.; Petroff, P.; Firouzi, A.; Janicke, M.; Chmelka, B. F. *Science* **1993**, *261*, 1299−1303.
(5) Huo, Q.; Margolese, D. I.; Stucky, G. D. *Chem. Mater.* **1996**, *8*, 1147.
(6) Ying, J. Y.; Mehnert, C. P.; Wong, M. S. *Angew. Chem., Int. Ed.* **1999**, *38*, 56−77.
(7) Dabbs, D. M.; Aksay, I. A. *Annu. Rev. Phys. Chem.* **2000**, *51*, 601−622.
(8) Novak, B. M. *Adv. Mater.* **1993**, *5*, 422−433.
(9) Baney, R. H.; Itoh, M.; Sakakibara, A.; Suzuki, T. *Chem. Rev.* **1995**, *95*, 1409−1430.
(10) Zhang, Z.; Tanigami, Y.; Terai, R. *J. Non-Cryst. Solids* **1995**, *189*, 212−217.
(11) Judeinstein, P.; Sanchez, C. *J. Mater. Chem.* **1996**, *6*, 511−525.
(12) Loy, D. A.; Shea, K. J. *Chem. Rev.* **1995**, *95*, 1431−1442.
(13) Shea, K. J.; Loy, D. A. *Chem. Mater.* **2001**, *13*, 3306−3319.
(14) Loy, D. A.; Baugher, B. M.; Baugher, C. R.; Schneider, D. A.; Rahimian, K. *Chem. Mater.* **2000**, *12*, 3624−3632.
(15) Matejka, L.; Dukh, O.; Hlavata, D.; Meissner, B.; Brus, J. *Macromolecules* **2001**, *34*, 6904−6914.
(16) Stein, A.; Melde, B. J.; Schroden, R. C. *Adv. Mater.* **2000**, *12*, 1403−1419.
(17) Sayari, A.; Hamoudi, S. *Chem. Mater.* **2001**, *13*, 3151−3168.
(18) Hoffmann, F.; Cornelius, M.; Morell, J.; Froba, M. *Angew. Chem., Int. Ed.* **2006**, *45*, 3216−3251.
(19) Zub, Y. L.; Seregyuk, I. V.; Chuiko, A. A.; Jaroniec, M.; Jones, M. O.; Parish, R. V.; Mann, S. *Mendeleev Commun.* **2001**, 1−3.
(20) Burleigh, M. C.; Markowitz, M. A.; Spector, M. S.; Gaber, B. P. *J. Phys. Chem. B* **2001**, *105*, 9935−9942.
(21) Rao, M. S.; Gray, J.; Dave, B. C. *J. Sol−Gel Sci. Technol.* **2003**, *26*, 553−560.
(22) Wahab, M. A.; Kim, I.; Ha, C. S. *J. Solid State Chem.* **2004**, *177*, 3439−3447.
(23) Wen, J.; Wilkes, G. L. *Chem. Mater.* **1996**, *8*, 1667−1681.
(24) Rankin, S. E.; McCormick, A. V. *Chem. Eng. Sci.* **2000**, *55*, 1955−1967.
(25) Kay, B. D.; Assink, R. A. *Mater. Res. Soc. Symp. Proc.* **1986**, *73*, 157−164.
(26) Yoon, H.-S.; Park, H.-S.; Kim, S.-H. *J. Korean Inst. Chem. Eng.* **1994**, *32*, 557−565.
(27) Sefcik, J.; McCormick, A. V. *Catal. Today* **1997**, *35*, 205−223.
(28) Assink, R. A.; Kay, B. D. *J. Non-Cryst. Solids* **1988**, *99*, 359−370.
(29) Sanchez, J.; McCormick, A. *J. Phys. Chem.* **1992**, *96*, 8973−8979.
(30) Inagaki, S.; Guan, S.; Fukushima, Y.; Ohsuna, T.; Terasaki, O. *J. Am. Chem. Soc.* **1999**, *121*, 9611−9614.
(31) Asefa, T.; MacLachan, M. J.; Coombs, N.; Ozin, G. A. *Nature (London)* **1999**, *402*, 867−871.
(32) Zhu, H. G.; Jones, D. J.; Zajac, J.; Dutartre, R.; Rhomari, M.; Roziere, J. *Chem. Mater.* **2002**, *14*, 4886−4894.
(33) Hunks, W. J.; Ozin, G. A. *Chem. Mater.* **2004**, *16*, 5465−5472.
(34) Burleigh, M. C.; Jayasundera, S.; Thomas, C. W.; Spector, M. S.; Markowitz, M. A.; Gaber, B. P. *Colloid Polym. Sci.* **2004**, *282*, 728−733.
(35) Liang, Y. C.; Hanzlik, M.; Anwander, R. *J. Mater. Chem.* **2005**, *15*, 3919−3928.
(36) Hunks, W. J.; Ozin, G. A. *J. Mater. Chem.* **2005**, *15*, 764−771.
(37) Brinker, C. J.; Lu, Y. F.; Sellinger, A.; Fan, H. Y. *Adv. Mater.* **1999**, *11*, 579.
(38) Angelome, P. C.; Soler-Illia, G. J. D. A. *J. Mater. Chem.* **2005**, *15*, 3903−3912.
(39) Angelome, P. C.; Soler-Illia, G. J. D. A. A *Chem. Mater.* **2005**, *17*, 322−331.
(40) Etienne, M.; Walcarius, A. *Electrochem. Commun.* **2005**, *7*, 1449−1456.
(41) Hatton, B. D.; Landskron, K.; Whitnall, W.; Perovic, D. D.; Ozin, G. A. *Adv. Funct. Mater.* **2005**, *15*, 823−829.
(42) Nicole, L.; Boissiere, C.; Grosso, D.; Quach, A.; Sanchez, C. *J. Mater. Chem.* **2005**, *15*, 3598−3627.
(43) Ji, X. L.; Hu, Q. Y.; Hampsey, J. E.; Qiu, X. P.; Gao, L. X.; He, J. B.; Lu, Y. F. *Chem. Mater.* **2006**, *18*, 2265−2274.
(44) Attard, G. S.; Glyde, J. C.; Göltner, C. G. *Nature (London)* **1995**, *378*, 366−368.
(45) Lebeau, B.; Fowler, C. E.; Hall, S. R.; Mann, S. *J. Mater. Chem.* **1999**, *9*, 2279−2281.
(46) Yang, S.; Mirau, P. A.; Pai, C. S.; Nalamasu, O.; Reichmanis, E.; Pai, J. C.; Obeng, Y. S.; Seputro, J.; Lin, E. K.; Lee, H. J.; Sun, J. N.; Gidley, D. W. *Chem. Mater.* **2002**, *14*, 369−374.
(47) Sadasivan, S.; Fowler, C. E.; Khushalani, D.; Mann, S. *Angew. Chem., Int. Ed.* **2002**, *41*, 2151−2153.
(48) Yu, C. Z.; Fan, J.; Tian, B. Z.; Zhao, D. Y. *Chem. Mater.* **2004**, *16*, 889−898.
(49) Tan, B.; Rankin, S. E. *J. Phys. Chem. B* **2004**, *108*, 20122−20129.
(50) Flodström, K.; Wennerström, H.; Alfredsson, V. *Langmuir* **2004**, *20*, 680−688.
(51) Nakanishi, K.; Kanamori, K. *J. Mater. Chem.* **2005**, *15*, 3776−3786.
(52) Soler-Illia, G. J. A. A.; Innocenzi, P. *Chem.—Eur. J.* **2006**, *12*, 4478−4494.
(53) Bao, X. Y.; Li, X.; Zhao, X. S. *J. Phys. Chem. B* **2006**, *110*, 2656−2661.
(54) Babonneau, F.; Leite, L.; Fontlupt, S. *J. Mater. Chem.* **1999**, *9*, 175−178.
(55) Etienne, M.; Lebeau, B.; Walcarius, A. *New J. Chem.* **2002**, *26*, 384−386.
(56) Olkhovyk, O.; Pikus, S.; Jaroniec, M. *J. Mater. Chem.* **2005**, *15*, 1517−1519.
(57) Grudzien, R. M.; Grabicka, B. E.; Pikus, S.; Jaroniec, M. *Chem. Mater.* **2006**, *18*, 1722−1725.
(58) Zhu, H. G.; Jones, D. J.; Zajac, J.; Roziere, J.; Dutartre, R. *Chem. Commun.* **2001**, 2568−2569.
(59) Bernards, T. N. M.; Bommel, M. J. V.; Boonstra, A. H. *J. Non-Cryst. Solids* **1991**, *134*, 1−13.
(60) Osterholtz, F. D.; Pohl, E. R. *J. Adhes. Sci. Technol.* **1992**, *6*, 127−149.
(61) Sanchez, J.; Rankin, S. E.; McCormick, A. V. *Ind. Eng. Chem. Res.* **1996**, *34*, 117−129.
(62) Vainrub, A.; Devreux, F.; Boilot, J. P.; Chaput, F.; Sarkar, M. *Mater. Sci. Eng., B* **1996**, *37*, 197−200.
(63) Rankin, S. E.; Macosko, C. W.; McCormick, A. V. *AIChE J.* **1998**, *44*, 1141−1156.
(64) Vainrub, A.; Devreux, F.; Sarkar, M.; Palasz, P. D.; Burgess, A. N. *J. Sol−Gel Sci. Technol.* **1996**, *6*, 279−285.
(65) Pu, Z.; van Ooij, W. J.; Mark, J. E. *J. Adhes. Sci. Technol.* **1997**, *11*, 29−47.
(66) Pouxviel, J. C.; Boilot, J. P. *J. Non-Cryst. Solids* **1987**, *94*, 374−386.
(67) Kay, B. D.; Assink, R. A. *J. Non-Cryst. Solids* **1988**, *104*, 112−122.
(68) Rousseau, F.; Poinsignon, C.; Garcia, J.; Popall, M. *Chem. Mater.* **1995**, *7*, 828−839.
(69) Tan, B. Ph.D. Thesis. University of Kentucky, Lexington, KY, 2005.
(70) Zelent, B.; Nucci, N. V.; Vanderkooi, J. M. *J. Phys. Chem. A* **2004**, *108*, 11141−11150.
(71) Tejedor-Tejedor, M. I.; Paredes, L.; Anderson, M. A. *Chem. Mater.* **1998**, *10*, 3410−3421.
(72) Lenza, R. F. S.; Vasconcelos, W. L. *Mater. Res.* **2001**, *4*.
(73) Muroya, M.-a. *Colloids Surf., A* **1999**, *157*, 147−155.
(74) Piana, K.; Schubert, U. *Chem. Mater.* **1995**, *7*, 1932−1937.
(75) Lenza, R. F. S.; Vasconcelos, W. L. *Mater. Res.* **2001**, *4*, 175−179.
(76) Matsumoto, T.; Takayama, Y.; Wada, N.; Onoda, H.; Kojima, K.; Yamadac, H.; Wakabayashic, H. *J. Mater. Chem.* **2003**, *13*, 1764−1770.
(77) Capozzi, C. A.; Pye, L. D.; Condrate, R. A. *Mater. Lett.* **1992**, *15*, 130−136.
(78) Pouchert, C. J. *The Aldrich Library of FT-IR Spectra*; Aldrich Chemical Co.: Milwaukee, WI, 1985; Vol. 2.
(79) Loy, D. A.; Carpenter, J. P.; Alam, T. M.; Shaltout, R.; Dorhout, P. K.; Greaves, J.; Small, J. H.; Shea, K. J. *J. Am. Chem. Soc.* **1999**, *121*, 5413−5425.
(80) Rankin, S. E.; McCormick, A. V. *Magn. Reson. Chem.* **1999**, *37*, S27−S37.
(81) Okumoto, S.; Fujita, N.; Yamabe, S. *J. Phys. Chem. A* **1998**, *102*, 3991−3998.
(82) Delak, K. M.; Sahai, N. *Chem. Mater.* **2005**, *17*, 3221−3227.
(83) Leffler, J. E.; Grunwald, E. *Rates and Equilibria of Organic Reactions*; Dover: Mineola, NY, 1989.
(84) Iler, R. K. *The Chemistry of Silica*; Wiley: Hoboken, NJ, 1979.
(85) Pohl, E. R.; Osterholtz, F. D. In *Molecular Characterization of Composite Interfaces*; Ishida, H., Kumar, G., Eds.; Plenum: New York, 1985; p 157.
(86) Tourkey, A. R.; Abdel-Hamid, A. A.; Slim, I. Z. *Z. Phys. Chem. (Leipzig)* **1972**, *250*, 49−60.
(87) Tremillon, B. *Chemistry in Non-Aqueous Solvents*; D. Reidel: Boston, 1974.
(88) Canals, I.; Oumada, F. Z.; Roses, M.; Bosch, E. *J. Chromatogr., A* **2001**, *911*, 191−202.